IN-SITU OPTICAL MEASUREMENT OF THE RAPID Li INTERCALATION AND DEINTERCALATION DYNAMICS IN COLLOIDAL 2D LAYERED TiS_2 NANODISCS

A Thesis

by

JIAGENG REN

Submitted to the Office of Graduate and Professional Studies of
Texas A&M University
in partial fulfillment of the requirements for the degree of

MASTER OF SCIENCE

Chair of Committee,	Dong Hee Son
Committee Members,	Emile Schweikert
	Jaime Grunlan
Head of Department,	Simon North

May 2017

Major Subject: Chemistry

ABSTRACT

Due to weak interlayer interaction, layered materials have been employed to accommodate various species of guests for energy storage and properties' modulation. Combined with riveting opto-electronic characteristics introduced by dimensions' reducing, two-dimension semiconducting nanomaterials including nanosheets, nanoflakes, nanoplates and nanodiscs have attracted attentions for research on optical and electronic devices, electrical cell development and so on. For these topics, many compounds from transition metal chalcogenides are candidates. TiS_2 has been intensively tested for battery electrode material with acceptance of Li^+. The dynamics and optical properties of this guest-host couple has been investigated on 2D TiS_2 nanodiscs in this thesis.

First an electrochemical platform was assembled for controllable lithium intercalation and deintercalation. Those ion migration processes with the nanodiscs led to observable and reversible optical change. The optical change resulting from ion intercalation and electron reception was monitored in situ and analyzed as a beacon for ion diffusion. To perform the goals of electrochemical control and live optical measurement, the electrochemical platform was built in a cuvette. The lateral confined 2D TiS_2 nanodiscs were deposited as a thin film on a transparent and conducting substrate to be intercalated with lithium from the electrolyte. Appropriate electrode voltages were applied to test the cyclic behavior of 2D TiS_2 with Li^+ intercalation and deintercalation. The same voltage was applied using non-intercalant ions with a result

of small portion of absorption change, which addressed that major contribution of the optical change was from ion intercalation rather than surface electron acceptance.

Upon lithium intercalation and deintercalation, visible absorption was weakened and recovered reversibly. The absorbance change fraction at the most drastic wavelength was extracted and analyzed for dynamics examination. Besides reversible optical switching in TiS_2 nanodiscs film, the responding time component was extracted to be just a few seconds compared with several quarters and hours by similar thickness of MoS_2 thin film in larger dimension. The absorption change fraction was tested and fit through a simplified radial diffusion model to estimate an 'effective' diffusion coefficient. The result shared the same order of diffusion coefficient of Li in TiS_2 thin films and observation of Li in MoS_2 films.

DEDICATION

To my family and dearest friends

ACKNOWLEDGEMENTS

I would like to thank Dr. Dong Hee Son for his constant help and guidance in my research. His engineering yet artful managing skill of scientific research and everyday life is truly a life goal for me to achieve. I would also thank my committee members Dr. Schweikert, Dr. Grunlan for their valuable advice and time for my thesis, so as Dr. Sheldon. I appreciate my previous advisor, Dr. Batteas for his help, tolerance and time. It's a valued opportunity to study here at Department of Chemistry, Texas A&M University and I really cherish this chance. I thank all the department staff, especially Sandy Horton, for all the help in these years. I thank Dr. Perla Balbuena for the theoretical calculation part of my research. I'd also thank all my lab members, Yitong, Daniel, David, Oscar, Dr, Ho Jin and Dr. Yerok Park for so much help and many precious suggestions during my research alongside Dr. Spear and Mrs. Carpenter-Werke, mentors from my previous group. Studying abroad for years can be lonely and grueling but I never caved in by those haunting and negative feelings thanks to all the understanding, insight and support from my family and friends. I am sincerely grateful for all these good deeds and wish everyone the best.

TABLE OF CONTENTS

Page

LIST OF FIGURES

Page

LIST OF TABLES

Page

CHAPTER I

INTRODUCTION

To fulfill various needs of properties and functions, materials are being developed in a growingly diversified trend. Altering the size of materials is an important route of modifying and enhancing their properties. When one or more dimensions of materials downsize to nanometer level, it is known as nanomaterials and they may present unique optical, electronic or mechanical properties. These properties enrich selections for particular characteristics. For example, semiconductor nanomaterials can have intriguing properties compared with their bulk counterparts.[1-3] The energy levels of semiconductor nanomaterials can be quantized due to the quantum confinement effect.[4-6] Electron-hole pair, or exciton is created in semiconductor nanocrystals via excitation. Quantization of energy levels caused by confinement of charge carriers (excitons), leads to size dependent optical spectra and may activate new mechanisms for carriers' relaxation.[7] These tunable opto-electronic properties can be applied in opto-electronic devices, solar cell or detection in bio-systems.[8-13]

Besides size, shape and composition can also alter the properties of materials.[3, 5] Layered materials, like graphite, process strong intralayer interaction and much weaker interlayer interaction. The structural difference of layered materials in intra- and interlayer dimensions results in anisotropy of optical, thermal and mechanical properties.[14, 15] The composition of stacking layers can be conductors as graphite, semiconductors as MoS_2, insulators like BN or combination of heterogeneous layers[16, 17].

Transitional metal chalcogenides are a wide type of layered materials that have been extensively researched. Constructing with transitional metals and chalcogenides as oxygen, sulfur, selenide and telluride, transitional metal chalcogenides in bulk are usually semiconductors while varying numbers of layers can lead to electronic transition. For instance, MoS_2 enjoys an indirect band gap of 1.23 eV in bulky crystal.[18] When reached monolayer, the indirect bandgap of MoS_2 undergoes a transition to a direct bandgap of 1.90 eV[19, 20].

The weak van der Waals gap of layered material enables properties' modification by intercalation. This suggests that modification of layered materials can be achieved by introducing various guests into the layered host structure. For layered transitional metal chalcogenides, optical, thermal and mechanical properties can be altered with introduction of atoms, ions, molecules and even layers. For example, the color of Bi_2Se_3 nanoribbon changed when high densities of copper atoms were introduced.[21] As TiS_2 was intercalated by selective organic molecules, the thermal conductivity of the modified TiS_2 were reduced by two orders than the single layer and bulk TiS_2 and might find application in wearable electronics[22, 23].

TiS_2 is a typical layered metal dichalcogenide. Each TiS_2 layer consists of an extensive sandwiched S-Ti-S structure in 1T phase. It has a layer distance of 57 pm[23] that accommodates various kinds of guests[22-26]. As a conducting material, the early research and application of TiS_2 was as cathode for batteries.[27, 28] TiS_2 was chosen due to being the lightest and cheapest of all transition metal dichalcogenide. The earliest

composition of rechargeable batteries with TiS_2 used Li metal as anode dated back to 1973.[28] Even though it showed reversibility of the battery reaction[28], the setup was ruled out for safety issues. In 1990s, TiS_2 was replaced by other cathode materials in rechargeable batteries. Still, TiS_2 is of interest in all-solid-state rechargeable batteries. Ball-milled, nanosized-TiS_2 was used to build a high power battery. [29] Chemical deposited, nanocrystalline TiS_2 was covered to encapsulate LiS_2. This nanocomposite showed high capacity as a cathode.[30]

Even though TiS_2 is currently not widely used as a cathode material, the extensive research shows advantage of lithiation of TiS_2: the process is reversible; the TiS2 structure is stable in the $0 \leq x \leq 1$ range of Li_xTiS_2 and free from phase transition.[26, 31] This suggests that lithiation of TiS_2 may be suitable for continuous tuning.

The Li-intercalated TiS_2 is reported to have less electrical resistance[32] and more transmittance in visible range[33], which enables observation of lithiation in optical and electrical change. The common lithiation methods include the use of lithium metal or n-butyl lithium. Both agents require low oxygen and humidity environment with careful operations. Even so, the lithiation with n-butyl lithium was reported to be violent and shred TiS_2 layers.[34] It can be very helpful to find a mild method to controllably intercalate lithium ions into TiS_2. Besides high power, nanosized TiS_2 is also expected to show faster dynamics of lithiation with reduced lateral dimensions. Apart from mechanically milling, solvent synthesis can also produce nanosized TiS_2, which have controlled and confined lateral sized and thickness.[35]

In summary, the goal is to set up a platform, which can mildly intercalate Li into TiS_2 nanodiscs and observe the in-situ optical change from intercalation. In this fashion, the recorded dynamics of optical change can be used to test the ion transport inside TiS_2 nanodiscs.

The thesis is organized as follows. Chapter II is a brief summary of necessary literatures. Chapter III introduces the experimental procedure to build the platform and measurement. Chapter IV is about the observation, analysis and discussion of dynamics of the intercalation and deintercalation of lithium into layered two dimensional TiS_2 nanodiscs. Finally, Chapter V discusses future aspects of the study.

CHAPTER II

BRIEF DISCUSSION ABOUT RELEVANT LITERATURES

2.1 The major differences between TiS_2 and lithiated TiS_2

2.1.1 Structural difference

Usually TiS_2 takes 1T phase, which Ti centers are coordinated by S ligands octahedrally.[36] After lithium ions enters the van der Waals gap of TiS_2 layers, the phase of lithiated TiS_2 remains. Although there is no phase transition with introduction of lithium, the interlayer distance expands from 57 pm to about 62 pm to accommodate foreign Li ions in bulk TiS_2.[27] The interlayer distance of TiS_2 corresponds to the 5 pm increase to *c*-axis in crystal parameters. In *a*-axis, the parameter slightly increase from 34.1 pm to 34.6 pm.[26] The lithiation of TiS_2 comes with injection of electrons to the structure, reducing Ti^{4+} to Ti^{3+} (instead of the reducing from Li^+ to Li atom). The slight increase of radii of Ti cations leads to minor expansion for *a*-axis.

Structural changes of TiS_2 nanodiscs with average radii of 50 nm were also conducted and measured.[26] These TiS_2 synthesized via solution methods showed an mild increment from 58.0 pm to 59.3 pm in *c*-axis (also the interlayer distance) and *a*-axis barely changed during the lithiation.

The lack of phase change and small structural change during lithiation and delithiation processes in TiS_2 nanodiscs helps the Li ion migration in the crystal and enables reversible intercalation and deintercalation.

2.1.2 Optical differences

The optical differences for TiS_2 and lithiated TiS_2 are from the electronic filling and carrier density change. The major visible absorption for TiS_2 is from the interband excitation of electrons in p-orbital to various d-orbitals[33] peaking around 2 eV. With lithiation, the peak would shift to a higher-energy range and the intensity around 2 eV would decrease.[33] This can be explained by Rigid Band Model, which supposed that the excess electrons alter the orbital fillings other than the position (energy) of these electronic bands.[33] Since Ti cations receive electrons with Li intercalation, the empty d-orbitals in TiS_2 is partially filled and this actually elevates the Fermi level, suppresses the interband transition and may increase the indirect bandgap. In lower energy region (< 1 eV), the free-carrier absorption (plasmonic) appears in the intercalated TiS_2 spectra due to extra electron density.[33]

2.1.3 Electronic properties

With lithiation, the electron concentration increases from 1.4×10^{20} cm^{-3} in pure TiS_2 to up to 2.2×10^{22} cm^{-3} in $LiTiS_2$ (x=1).[37] The increased electron concentration is also clearly seen in the resistivity. The resistivity falls drastically with growing x in the Li composition.[37] $LiTiS_2$ shows a resistivity about two orders below than that in TiS_2. So with introduction of Li, TiS_2 may switch from a semi-conducting behavior to metallic behavior upon enough Li introduction.

2.2 Determination of Li transport in TiS_2

Since TiS_2 was first investigated as a cathode material, characteristics like the Li^+ diffusion coefficient between TiS_2 van der Waals gaps were determined to evaluate the performance for potential battery application back in 1980s and 1990s. The major methods can be categorized into two types: chemical diffusion coefficient and spin lattice relaxation in Li_xTiS_2.[38, 39] Chemical diffusion is required by analysis of electrochemical data based on the lithiation process into pure TiS_2 via Li metal-TiS_2 battery, while spin lattice relaxation is based on NMR investigation of Li^+ motion frequency in crystal of already lithiated TiS_2. The reported data of Li diffusion coefficient (*D*) is summarized in Table 2.1 for more detailed classification of measuring method.

Table 2.1 Summary of selective reported Li diffusion coefficient (*D*) values and respective methods

Types	Technique	Forms of sample	*D* ($\times 10^{-9}$ cm^2/s)
Chemical	potentiostatic	TiS_2 single crystal	10 ([40])
Chemical	chronoamperometry	3-10 μm TiS_2 grain	1.5 ([41])
Chemical	Current-pulse	TiS_2 single crystal film (6 mm size and 60 μm thickeness	A maximum of 6~100 ([42])
Chemical	Current-pulse	TiS_2 thin films	10^{-4} ~ 10^{-3} ([43])
Chemical	AC impedance	TiS_2 powder	8.1 $\times 10^{-3}$ ([44])
NMR relaxation		$LiTiS_2$	1 ([45])

The reported data in Table 2.1 vary by several orders of magnitude. The differences can be addressed by assumptions in different methods, differences in the form of TiS_2 and experimental conditions.[44] In general, the higher *D* values are related with the side reactions and non-Faraday reactions (for example, residual current) on the electrodes. The excess Ti from sample preparation also leads to a varying range of *D*.[42]

2.3 Optical observation of MoS_2 nanosheets upon ion intercalation

As another layered transition metal chalcogenide, MoS_2 is under extensive research especially for 2D material[46]. Even though the common coordination of the metal center differs, MoS_2 and TiS_2 have been both investigated for opto-electronic devices, electrical energy storage and other similar potential applications. The reported change, properties and mechanisms of intercalation in MoS_2 is helpful to understand similar process in TiS_2.

2.3.1 Control of optical properties in MoS_2 nanosheets with ion intercalation

Similar to TiS_2, lithiation of MoS_2 results in enhancement of optical transmission and electrical conductivity led by filling of electrons and elevating of fermi level. The photoluminescence (PL) of 2D MoS_2 nanoflakes was modulated via intercalation and deintercalation of Li, Na and K.[47] The intensity of PL of MoS_2 nanoflakes was reduced upon the intercalation due to Fermi level elevating and excitation suppression. Deintercalation process was demonstrated to recover the PL intensity. The response time

of the PL intensity modulation and recover was around a couple of ten seconds given the typical size of 50~100 nm and a majority of only a few monolayers.

Inspired by the modulation of optical properties with ion intercalation, a platform was assembled for tuning optical and electronic properties with Li intercalation in MoS_2.[48] The ultrathin film of MoS_2, with 20-35 nm thickness and 5~20 μm size, underwent electrochemical control of lithiation and delithiation. The increased transmission and recovery duration was around 40 minutes. In contrast, the lithiation of another appropriate-size MoS_2 film using n-butyl lithium took more than two hours.

2.3.2 Visualization of ion transport in MoS_2

The structural change of layered material can be used to estimate transport rate of ions. For bulk TiS_2, the 10% interlayer distance expansion is larger enough to locate the boundary of lithiation.[41] But small changes in TiS_2 nanodiscs make it much harder to observe the change and there is no report of local visualization in TiS_2 nanodiscs so far.

Unlike TiS_2, MoS_2 does bear the generation of nucleation of a new phase under lithiation. The origin 2H (each Mo ion is surrounded by six S ions in trigonal prismatic arrangement) would transform to 1T (still six S ions, but in octahedral arrangement). This phase transition results in obvious boundary between pure and lithiated MoS_2, allowing direct observation and estimation of ion transport in nanocrystals.

Bai et al. reported atomic visualization of electrochemical lithiation process of MoS_2 nanosheets.[49] It was observed that there was a clear boundary between two compositions of MoS_2 under TEM. This observation inspired Gao et al.[50] When the

electrochemical process of lithiation was captured over time, the boundary between two phases spread. By calculating the enlargement of lithiated area within given time range, the diffusion coefficient of lithiation of MoS_2 nanosheets was estimated. Gao reported the diffusion rate of lithiation as 30-70 nm/s with data reported by Bai. The idea of estimation via area change was also applied to the sodiation of MoS_2 nanosheets. Gao reported sodiation rate in MoS_2 as 3-7 nm/s, about one order slower than lithiation.

Aside from TEM, the full cycle intercalation and deintercalation of lithium ion in MoS_2 is recently reported via optical microscopy. [51] Though atomic details of lithiation was revealed via electrochemical STM and AFM, the uncovered results were more about the initial stage of lithiation yet a complete cycle.[52, 53] A laser confocal microscope combined with a differential interference contrast microscope (LCM-DIM) was developed and can reach atomic resolution on metal electrodes. Upon lithiation, the phase difference and absorption change leads to new domains captured by LCM-DIM. It also shows the layer by layer intercalation via in-situ visualization.[51]

CHAPTER III

EXPERIMENTAL METHODS*

3.1 Synthesis of TiS_2 nanodiscs

TiS_2 nanodiscs were synthesized by reported solution method.[35] Briefly, the synthesis was adding sulfur source (CS_2) into the mixture of titanium source ($TiCl_4$) and oleyamine (also helps dispersion) at 300 °C. The size of TiS_2 nanodiscs was controlled by the concentration of sulfur and titanium precursors. The chemical reaction is described as below:

$$CS_2 + RNH_2 \rightarrow H_2S + RNCS \ (R= CH_2(CH_2)_7CH=CH(CH_2)_8)$$

$$TiCl_4 + 2H_2S \rightarrow TiS_2 + 4HCl$$

The method produces well defined colloidal nanodiscs. In this and next chapter, the experiment steps apply to mainly *r*=80 nm and *r*=250 nm samples.

3.2 Fabrication of TiS_2 film on ITO

3.2.1 Photoinduced separation of TiS_2 nanodiscs

The synthesized TiS_2 nanodiscs were stacks of well-defined shape and size. However, those stacks may aggregate and assemble. The assemblies of TiS_2 stacks lead to uncertain thickness. For even distribution of TiS_2 stacks on substrate, TiS_2 colloidal

---

* Reprinted in part with permission from Ren, Jiageng, Camachi-Forero, Luis; Rossi, Daniel; Park, Yerok; Balbuena, Perla; Son, Dong Hee. In situ optical measurement of the rapid Li intercalation and deintercalation dynamics in colloidal 2D layered TiS_2 nanodiscs. *Nanoscale* **2016,** *8,* 11248-11255. Copyright 2016 by the Royal Society of Chemistry.

solution was photo-separated to single stacks (each stack of TiS_2 nanodiscs still contains multiple TiS_2 layers) before film fabrication.

TiS_2 from section 3.1 were dispersed in deoxygenated chloroform with pulsed laser at 800 nm for photoseparation.[54] Constant stirring was required during the whole process. The basic mechanism to separate those 2D colloidal materials is utilizing the anisotropy. The pulsed laser alters the transient charge distribution of TiS_2 nanodiscs. When the modification of charge distribution is sufficiently large to weaken the interparticle forces between stacks, solvent molecules can take advantage of pulsed laser and facilitate the solvation of each single nanodiscs stack.

3.2.2 Cleaning of the deposition substrate

ITO glass was used as the substrate for TiS_2 deposition due to its transparency and conducting nature. The ITO glass was cut into slides of about 0.9 centimeters wide and 3.8 centimeters long. ITO was coated on only one side of the slides, thus necessary to mark the ITO side on the edges that would not influence following procedures and measurements. The cut and marked slides were immersed in boiling acetone for five minutes and later rinsed with methanol. Then these slides were sonicated in methanol for five minutes. After sonication, the slides were dried with nitrogen gas, and got UV-ozone cleaned for an hour. During the UV-ozone cleaning, the slides were placed with the glass side, ITO side facing up, not in contact with the holder. The UV-ozone treated slides were immediately used for TiS_2 deposition. Some of the slides were kept without subsequent deposition, used as reference electrode for later optical measurement.

3.2.3 Deposition of TiS_2 nanodiscs

Better dispersed TiS_2 nanodiscs solutions from 3.2.1 were soon used for TiS_2 deposition after the photoexcitation separation steps. The concentration of TiS_2 solution was adjusted based on the absorption, to 0.5~1.5 in 1 centimeter wide cuvette. This concentration range was selected for better separation efficiency and consequent deposition. It produced a nicely deposited, homogenous optical thin film on the surface. Trials of higher concentration for deposition were made, resulting in films with higher absorption, inhomogeneous look with stacked region.

The TiS_2 solution was sonicated briefly before the deposition. After sonication, the UV-ozone treated slides were put in the solution with about 3 centimeters of the slides immersed in solution and 0.8 centimeter blank for deposition. The blank part was in contact with alligator clips for cell assembly later, so no need for TiS2 deposition. The container with solution and slides was sealed and kept still and undisturbed for twelve hours.

After twelve hours, the slides were rinsed with excessive deoxygenated chloroform to remove loosely attached TiS_2. Both faces of the slides were coated with TiS_2, and the deposition on the bare glass side was wiped with ethanol damped cotton swabs. After visible deposition was removed, the side was wiped once more with ethanol damped cotton swabs. The slides were rinse with excessive ethanol to remove unexpected cotton contamination after each wipe. Then the slides were dried with nitrogen flow and ready for cell assembly.

Unused TiS_2 slides were kept in a clean and dry container. The container with slides was purged with argon so the slides were kept under inert atmosphere. Fig. 3.1(a) shows the AFM image of TiS_2 film and the profile for one TiS_2 nanodisc with an average radii and height of 80 nm and 15 nm respectively. Fig 3.1(b) is the optical absorbance of this film. The inset of Fig. 3.1(b) is the optical image of the TiS_2 coated part with respect to the absorption of Fig. 3.1(b).

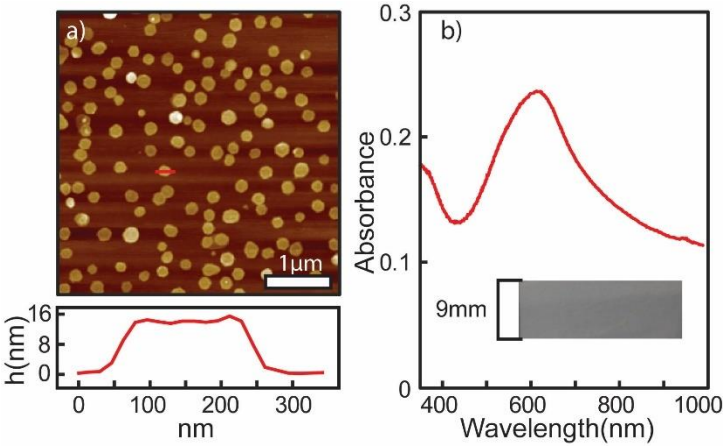

Figure 3.1 (a) AFM images of TiS_2 nanodiscs deposited on ITO/glass. (b) Absorption spectrum and photograph of the TiS_2 nanodisc film.

3.3 Assembly of the cell

The cell was assembled as Fig 3.2 shows. The cell was set up in a rectangular cuvette to facilitate the optical measurement. The TiS_2-ITO/glass was working electrode, with uncoated end in contact with the potential stat. A silver wire in electrolyte with glass tube protection was pseudo-reference electrode. And the carbon cloth was as the counter electrode. For easier connection, a platinum wire was connected to the carbon

cloth and actually in contact with the potential stat. The carbon cloth was electrochemically cleaned before in use to remove interfering carbon groups. The electrolyte was usually 0.1 M $LiClO_4$ in acetonitrile unless specified in other electrolytes or concentrations. The reference for the absorption measurement was a clean blank ITO-glass slide without the deposition of TiS_2 in 0.1 M $LiClO_4$ or the same electrolyte solution if specified, using the same type of rectangular cuvette. Both sample and reference cuvettes were put on a cover and sealed immediately to inhibit evaporation of volatile solvent.

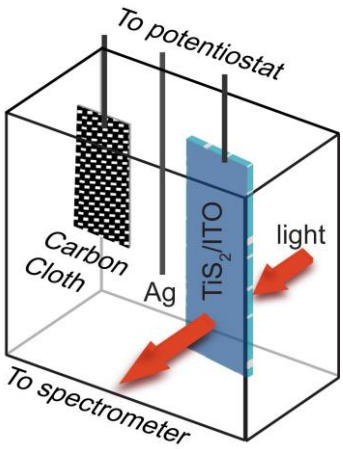

Figure 3.2 Setup for the optical measurement of electrochemical Li intercalation dynamics in TiS_2 nanodiscs

The apparatus not shown on the Fig. 3.2 was a spacer occupies the lower part of the cuvette. The slit for positioning TiS_2/ITO electrode (or the reference ITO) and hole for pseudo-reference were intentionally carved and aligned with the respective parts in the cover. The spacer alone can take up the space, reduce the use of chemical and

position the electrodes. The cooperation of spacer and the cover helped to mount and secure the position of electrodes, especially the TiS_2/ITO electrode, whose position would be sensitive for absorption measurement.

The Ag wire pseudo reference was calibrated with results as Fig. 3.3. The calibration cell was set up with glassy carbon working electrode, Pt wire as counter electrode, and the to-be-calibrated Ag pseudo reference electrode. 1×10^{-4} M ferrocene in 0.1 M $LiClO_4$ acetonitrile solution was the electrolyte. Ferrocene works as the inner reference to calibrate the Ag wire pseudo reference. The shape of curve and peak positions of reduction and oxidation was stable over 14 cycles, which means the Ag wire pseudo reference was stable and competent as a reference electrode.

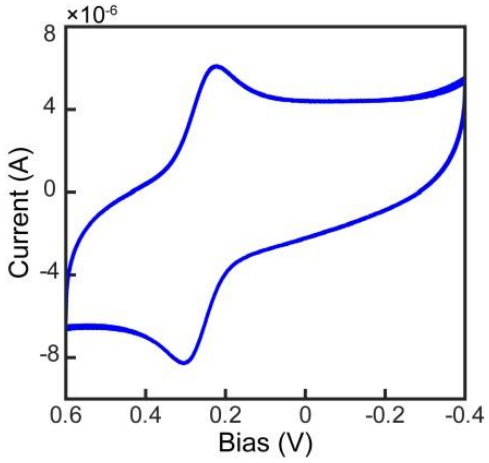

Figure 3.3 Calibration curve of Ag wire pseudo reference of 14 cycles

The reported potential of ferrocene (Fc^+/Fc) over standard hydrogen electrode (SHE) is 0.62 V[55]. Deducted by 0.25 V, the average potential of reduction and oxidation peak, the Ag pseudo reference was around 0.37 V over SHE.

3.4 Optical measurement of TiS_2 under potential

3.4.1 Basic setup for a single spectrum measurement

The data were exacted from the absorption spectra. The sample was assembled as description of section 3.3. The reference was based on cleaned ITO/glass without deposition of TiS_2 films. Then the blank ITO/glass was immersed in the same batch of electrolyte solution of the sample also in 1 centimeter wide cuvette.

The absorption measurement ranges from UV-Vis range to near-IR range (400-1600 nm) with halogen lamp as the light source. A CCD detector (QE 65 pro, ocean optics) was used to acquire the UV-vis range (400-950 nm) while a home-built spectrometer in dual beam configuration was used to measure the near-IR region (900-1600 nm). The overlap helped correct and combine the spectrum.

Using the CCD detector, the reference data was measured and set before the sample data. The spectrometer for near-IR compared the data from the reference and sample simultaneously via two InGaAs detector.

3.4.2 Continuous measurement of optical spectra

The measurement was conducted based on continuous output of absorption measurements. To acquire dynamic change of TiS_2 under potential applying in visible range, the data was set to be automatically exported in every 0.25 seconds, which also set the time resolution of the experiment. The time resolution was chosen to discover optical dynamics within seconds and average enough to reduce spectrometer fluctuation.

The potential stat was responsible for electrical bias applying and current-time data collecting. The time frame for the data export was preset to cover all stages. In a typical cycle, there was a negative electrical bias stage (typically -1.1 V vs Ag pseudo-reference electrode), a relative positive electrical bias stage (typically 0.3 V vs Ag pseudo-reference electrode) and an optional no potential (open circuit) stage. For samples in different sizes, the duration of the stages under electrical bias varied: usually 150 s for r=80 nm sample and 300 s for r=250 nm sample. The I-V data on the working electrode, TiS_2 film, was also collected.

The time resolution of near-IR region is more than a couple of seconds and not nearly as good as the visible range. Therefore the spectra in near-IR region were usually used for stable status like before and after intercalation and not for following dynamics interpretation. For example, multiple spectra after intercalation were acquired and compared, only the spectrum indicating stable status was used to represent “after intercalation”. The time frame of the measurement was the same as visible range measurement.

3.4.3 Blank test

The bare ITO/glass was tested under given experimental voltages as mentioned in 3.4.2. It can help confirm that the contribution of optical change by only ITO/glass substrate under electrical bias is neglectable. As Fig. 3.4 shows, there was absence of absorbance change under -1.1 V, 0.3V (both vs Ag pseudo reference) and open circuit

range confirming that ITO does not contribute to absorbance change under experimental voltage range.

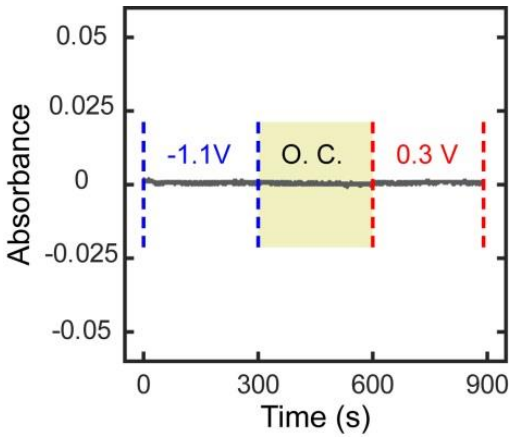

Figure 3.4 Absorption value of ITO/glass at 600 nm at -1.1 V and 0.3V vs Ag pseudo reference electrode

3.5 Data analysis

3.5.1 ΔA(*t*)/A extraction

A contrast of TiS_2 film spectra before and after lithium intercalation is shown as Fig. 3.5. The major differences are the decreasing absorption intensity around 600 nm and the onset >1400 nm after lithium intercalation. Based on the time resolution of data in these two regions, absorption at 600 nm was selected as the representative of the optical change. For further data analysis, absorbance at 600 nm at difference time are extracted and compared. To compare between films, the ratio of absorption decline, ΔA/A, was used instead the value of absorption. In this way, the dynamics of optical

change was set at the real-time fraction change of original film absorption at 600 nm, $\Delta A(t)/A$.

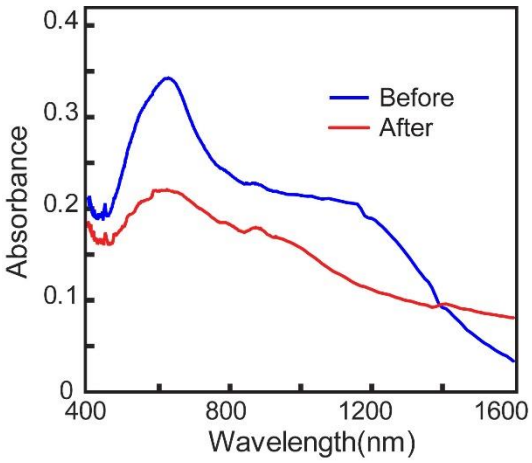

Figure 3.5 Absorption spectra of the TiS_2 nanodisc film before and after Li intercalation.

3.5.2 Bi-exponential fitting of $\Delta A(t)/A$

Fitting and acquiring suitable parameters from $\Delta A(t)/A$ can help compare behavior of film and dynamics of different sizes of TiS_2 nanodiscs. Through bi-exponential model:

$$\frac{\Delta A(t)}{A} = A_1 \exp\left(-\frac{t}{\tau_1}\right) + A_2 \exp\left(-\frac{t}{\tau_2}\right) + c$$

time components of $\Delta A(t)/A$ were extracted. A sample of fitting via bi-exponential model is shown as Fig. 3.6.

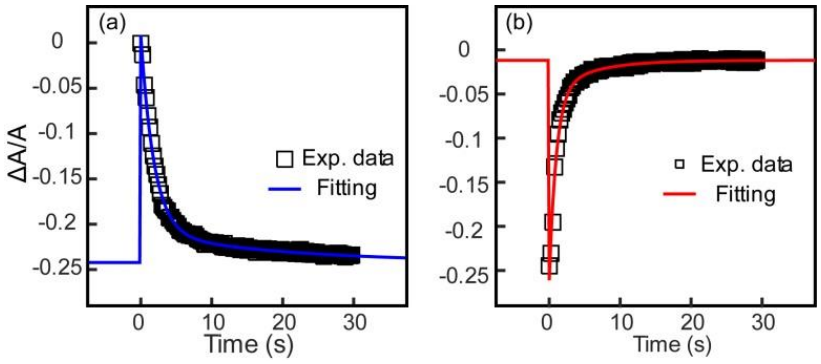

Figure 3.6 Fitting of ΔA(*t*)/A with bi-exponential model for *r*=80 nm sample at (a) -1.1V and (b) 0.3V.

CHAPTER IV

IN-SITU OPTICAL MEASUREMENT OF THE RAPID LI INTERCALATION AND DEINTERCALATION DYNAMICS IN COLLOIDAL 2D LAYERED TIS_2 NANODISCS[*]

4.1 Introduction

In the past years, progress in fabricating atomically thin 2-dimensional (2D) transition metal dichalcogenide (TMC) materials with controllable thickness enabled the observation of various unique optical and electronic properties tunable by controlling the number of the layers. For instance, indirect to direct bandgap transitions are observed in many semiconducting TMCs when the thickness reaches a single layer.[19, 56-58] Nonlinear optical properties, such as second harmonic generation,[59, 60] are also changed by varying the thickness. These thickness-tunable optical properties of thin layered TMC materials are obtained from the dependence of the interlayer electronic interaction or symmetry with varying number of the layers.[61, 62] Recently, several studies showed that intercalation of metal ions, which has been utilized to tune the properties of various layered or porous materials, can also be used to modify the optical and electronic properties of the atomically thin layered TMC. For instance, the optical transmission and electrical conductivity have been varied via Li intercalation in MoS_2 films

[*] Reprinted in part with permission from Ren, Jiageng, Camachi-Forero, Luis; Rossi, Daniel; Park, Yerok; Balbuena, Perla; Son, Dong Hee. In situ optical measurement of the rapid Li intercalation and deintercalation dynamics in colloidal 2D layered TiS2 nanodiscs. *Nanoscale* **2016,** *8,* 11248-11255. Copyright 2016 by the Royal Society of Chemistry

demonstrating their potential to obtain dynamically controllable optical and electronic properties.[48, 63]

Because the intercalation in the layered TMC involves highly anisotropic diffusion confined to the interlayer van der Waals gaps, the lateral dimension is a key factor determining the time scale of intercalation. Therefore, slow intercalation in large-area TMC films, such as those fabricated from CVD taking minutes or longer depending the area, can be an issue when the fast dynamic control of the properties is desired. In this regard, chemically-synthesized colloidal layered TMC nanodiscs can be an ideal platform to gain the rapid modulation of intercalation-induced material properties, since their lateral size can be varied in the nanoscale providing much shorter distance for the diffusion of the intercalants.[35, 64]

Here, we fabricated thin films of colloidal TiS_2 nanodiscs, composed of well-separated nanodiscs deposited on ITO/glass surface, as the platform to investigate the rapid dynamic control of the material properties of TMC via intercalation at nanoscale lateral dimension. With these films, the dynamics of electrochemical Li intercalation and deintercalation were measured via in-situ optical method taking advantage of the high optical homogeneity of the fabricated film and the dependence of the interband optical absorption of TiS_2 nanodiscs on Li intercalation. Unlike in chronoamperometry commonly used to monitor the metal intercalation,[41, 42] the optical probing can circumvent the complications from spurious Faradaic or non-Faradaic processes that can obscure the measurement of the intercalation/deintercalation dynamics. In this study, we

could readily measure the electrochemical Li intercalation and deintercalation dynamics occurring on second time scale in the films of TiS_2 nanodiscs of ~100 nm lateral dimension. In addition, the change of the rate and reversibility of the intercalation/deintercalation processes with the nanodisc size and during the multiple intercalation/deintercalation cycles could be observed providing a unique opportunity to study the dynamics of 2D intercalation and deintercalation in the layered TMC materials with nanoscale lateral dimension. Information obtained from this study will also be valuable for understanding the charging and discharging dynamics in batteries based on nanoscale layered materials.

4.2 Results and discussion

4.2.1 General change of absorption in TiS_2 nanodiscs by Li-intercalation

Fig. 3.5 shows the absorption spectra change for TiS_2 film of r=250 nm sample deposited on ITO/glass under -1.1 V (vs. Ag pseudo reference), ranging from 400 nm to 1600 nm. As mentioned in Chapter III, an obvious decrease of the intensity was noted for the interband absorption, centered at 600 nm upon the intercalation of lithium ion. The reaction on TiS_2 film is $TiS_2 + x\ Li^+ + x\ e^- \rightarrow Li_xTiS_2$. The change in the interband absorption spectrum by metal intercalation has been observed in several layered materials such as MoS_2[48] and Bi_2Se_3.[65] As explained in Chapter II, the optical absorption decrease is due to the increase of the optical bandgap. The filling of the conduction band with electrons, or the collapse of the bandgap from the overlap of the bandgap, results in

the optical bandgap.[34, 66] In the case of Li-intercalated TiS_2, electronic structure calculations suggested that the observed reduction of interband absorption originated from the overlap of conduction and valance band near the Fermi level.[36] This could also leads to the enhancement of metallic behavior of TiS_2.[36] In addition, the absorption at >1400 nm increased upon Li intercalation, which is considered to be due to the higher free carrier density and giving rise to the plasmon resonance.[33] This suggests that the possibility of utilizing colloidal TiS_2 nanodiscs is not only for optical transmissions but also plasmonic effects.

As the brief discussion in section 3.5.1, the fraction change of peak intensity of interband absorption near 600 nm, $\Delta A(t)/A$, was recorded to examine the dynamics of Li intercalation and deintercalation.

To optimize and control the condition for Li^+ ion intercalation, a few parameters were conducted. After basic parameters were controlled, like the size of the ITO/glass slides or absorbance of the TiS_2 film, the potential dependence of Li^+ ion intercalation was tested. The results of potential dependence between -0.5 V and -1.3 V (unless otherwise specified, the potential was in comparison with Ag wire pseudo reference) on r=250 nm sample were shown in Fig. 4.1. The general trend indicated that $\Delta A(t)/A$ increased from -0.5V to -1.1 V saturated starting from -1.1 V. Hence -1.1 V was chosen since it showed the saturation of the modulation amplitude of $\Delta A(t)/A$. More negative potential may increase the possibility of unwanted change like fastening the

deconstruction of the TiS_2 or reduction of some chemical agent. Likewise +0.3 V was chosen for the deintercalation potential, also considering the dynamics of deintercalation.

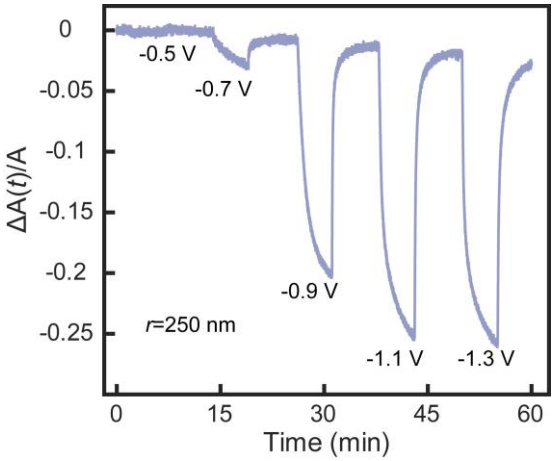

Figure 4.1 Dependence of $\Delta A(t)/A$ on the electrode potential measured in TiS_2 nanodiscs at r=250 nm

4.2.2 Dynamics of intercalation and deintercalation of *r*=80 nm and *r*=250 nm TiS_2 nanodiscs

First the dynamics of intercalation and deintercalation of samples of two different radii were discussed. Fig. 4.2(a,b) show the $\Delta A(t)/A$ over multiple cycles during alternating potential of -1.1 V and 0.3 V of samples of average radii of 80 nm and 250 nm respectively. Fig. 4.2 (d,e) are the magnified view of the first few seconds of certain applied voltages of both nanodiscs, featuring the most drastic stage of $\Delta A(t)/A$. At the onset of -1.1 V, there was a rapid decrease of $\Delta A(t)/A$ initially and following plateau afterwards. As the potential switches to -0.3 V, $\Delta A(t)/A$ recovered with the

deintercalation of Li. Samples of both radii exhibit qualitatively similar behavior of $\Delta A(t)/A$, while the dynamics was faster in the smaller sample as clearly seen in Fig. 4.2(d,e).

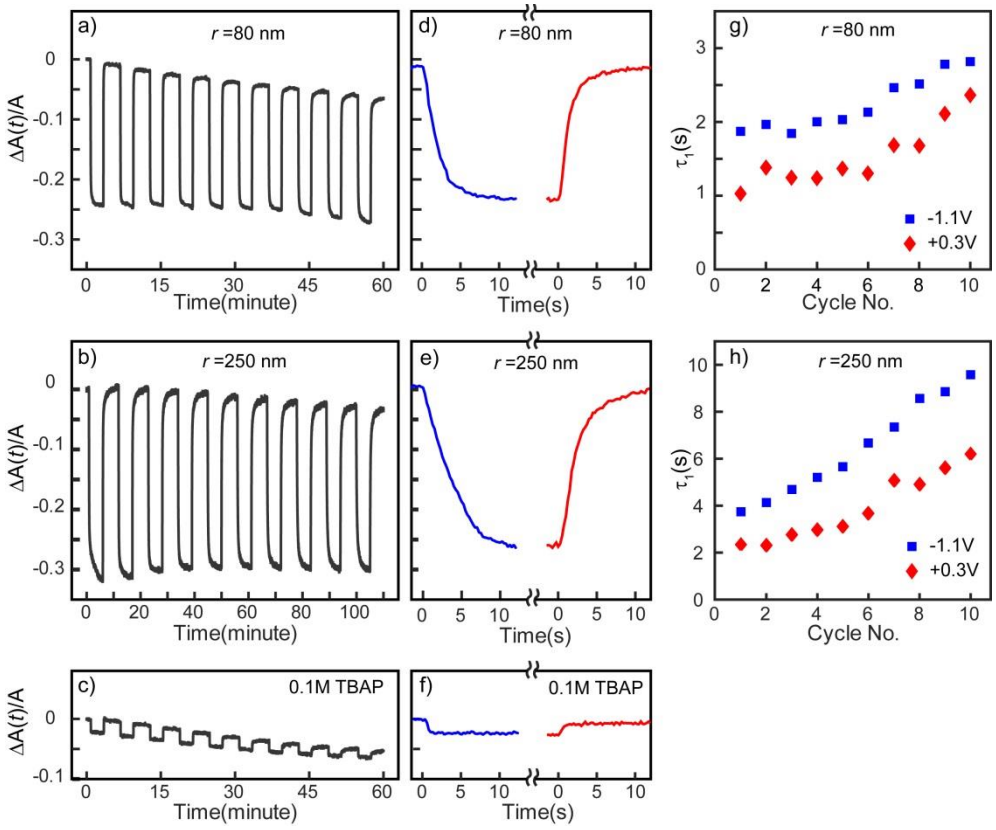

Figure 4.2 (a,b) $\Delta A(t)/A$ during the multiple cycles of potential step alternating between -1.1 V and 0.3 V in TiS_2 nanodiscs of r=80 nm (a) and r=250 nm (b). (d,e) Magnified view of $\Delta A(t)/A$ in one intercalation (blue) and deintercalation (red) cycle for TiS_2 nanodiscs with r=80 nm (d) and r=250 nm (e). (g,h) Time component (τ_1) for the intercalation and deintercalation process at each cycle for TiS_2 nanodiscs with r=80 nm (g) and r=250 nm (h). (c,f) $\Delta A(t)/A$ obtained with 0.1 M TBAP as the non-intercalating electrolyte in TiS2 nanodiscs with r=80 nm.

The possible contribution of the surface adsorption of the electrolytes to $\Delta A(t)/A$ was tested using tetrabutylammonium perchlorate (TBAP, 0.1 M) as the non-intercalating electrolyte in the absence of $LiClO_4$. The modulation amplitude of $\Delta A(t)/A$ by TBAP is less than 10% of what was observed under Li^+ intercalation and the dynamic response was much faster consistent with the surface process, as shown in Fig. 4.2 (f). Since the effect of the adsorption of electrolyte was minor, it was not taken into consideration of the analysis of $\Delta A(t)/A$ throughout the study.

A small decrease of the modulation amplitude and downward shift of $\Delta A(t)/A$ can be seen, with repeated intercalation/deintercalation cycle. This may reflect the change in chemical equilibrium at a given reference electrode potential. It may also refer to small irreversibility in the host structure that may introduce systematic changes in the absorption intensity. While the amplitude is an interesting issue deserving an additional study, the dynamics of intercalation and deintercalation is the primary focus in this chapter.

It is worth comparing $\Delta A(t)/A$ from the optical measurement and the amount of charge transferred measured via amperometry during the intercalation and deintercalation processes, which illustrates the advantage of the optical measurement. Fig. 4.3 compares $\Delta A(t)/A$ and the amount of the transferred charge ($Q(t)$-$LiClO_4$) in the presence of 0.1 M $LiClO_4$ during Li deintercalation step. The amount of charge transferred in the presence 0.1 M TBAP used as non-intercalating electrolyte ($Q(t)$-TBAP) is also shown. The dynamics reflected in $Q(t)$-$LiClO_4$ and $Q(t)$-TBAP are similar

and much slower than that of ΔA(*t*)/A. It is also notable that the magnitude of Q(t)-TBAP is significant despite the absence of the intercalation, indicating the susceptibility of the electrochemical probe to the potential interference from non-intercalating processes obscuring the interpretation of the intercalation and deintercalation dynamics.

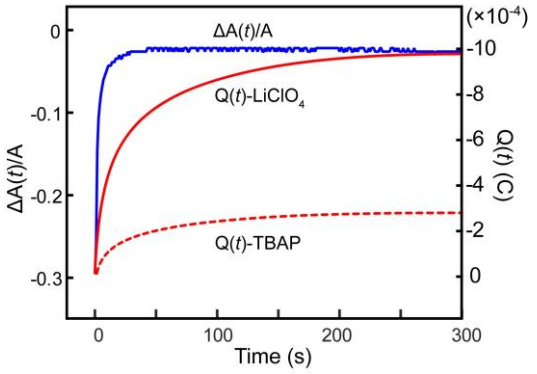

Figure 4.3 Comparison of ΔA(*t*)/A and charge flow (Q(*t*)-$LiClO_4$) for the deintercalation in TiS_2 nanodiscs with *r*=250 nm. Charge flow measured with 0.1 M TBAP (Q(*t*)-TBAP) is added for comparison.

For a more quantitative comparison of the dynamics of intercalation and deintercalation in the nanodiscs of different radius and also at different stages of the multiple potential cycle, ΔA(*t*)/A was fit to a biexponential function.

Here, a simple phenomenological model is used to extract and compare the timescales of the intercalation and deintercalation in TiS_2 nanodisc films. The fitting results are summarized in Table 4.1. Since the fast component carries the majority (typically 80-90%) of the amplitude in both the decay and recovery of ΔA(*t*)/A and its

time constant (τ_1) is well separated from that of the slow component (τ_2), τ_1 will be the focus for the comparison of the dynamics. Fig. 4.2(g, h) compare τ_1 of $\Delta A(t)/A$ for both the intercalation and deintercalation processes in the two TiS_2 nanodisc films during each intercalation/deintercalation cycle, which are on the order of seconds and decrease with the radius of the nanodiscs. The timescale of the intercalation in TiS_2 nanodiscs is similar to a couple of seconds with similar lateral dimension[47], and more than an order of magnitude shorter than minutes or longer required for the intercalation in other related TMD sheets with larger lateral dimensions (e.g., 5-20 μm)[48] . The data in Fig. 4.2 clearly show the advantage of the reduced lateral dimension of the nanodiscs in obtaining a rapid dynamic control of the material properties via 2-dimensional intercalation.

Table 4.1 Fitting parameter of $\Delta A(t)/A$ with biexponential function. The amplitudes (A_1 and A_2) are the fractional amplitudes.

For TiS_2 with r=80 nm

Cycle No.	Intercalation (-1.1V)					Deintercalation (0.3V)			
	A_1	τ_1 (s)	A_2	τ_2 (s)		A_1	τ_1 (s)	A_2	τ_2 (s)
1	0.87	1.9	0.13	20		0.85	1.0	0.15	5.6
2	0.94	2.0	0.06	132		0.92	1.4	0.08	8.9
3	0.96	1.8	0.04	39		0.93	1.2	0.07	11
4	0.96	2.0	0.04	59		0.92	1.2	0.08	11
5	0.94	2.0	0.06	42		0.91	1.3	0.09	10
6	0.92	2.1	0.08	26		0.91	1.3	0.09	16
7	0.91	2.5	0.09	30		0.92	1.7	0.08	22
8	0.89	2.5	0.11	26		0.89	1.7	0.11	28
9	0.87	2.8	0.13	29		0.89	2.1	0.11	28
10	0.85	2.8	0.15	33		0.89	2.4	0.11	32

Table 4.1 continued

For TiS_2 with r=250 nm

Cycle No.	Intercalation (-1.1V)					Deintercalation (0.3V)			
	A_1	τ_1 (s)	A_2	τ_2 (s)		A_1	τ_1 (s)	A_2	τ_2 (s)
1	0.75	3.8	0.25	1.2×10^2		0.84	2.4	0.16	50
2	0.88	4.1	0.12	64		0.81	2.3	0.19	43
3	0.89	4.7	0.11	36		0.81	2.8	0.19	46
4	0.86	5.2	0.14	37		0.80	3.0	0.20	44
5	0.84	5.7	0.16	51		0.78	3.1	0.22	43
6	0.79	6.7	0.21	50		0.78	3.7	0.22	46
7	0.78	7.4	0.22	52		0.81	5.1	0.19	48
8	0.76	8.6	0.24	53		0.78	4.9	0.22	48
9	0.71	8.9	0.29	52		0.76	5.6	0.24	47
10	0.68	9.6	0.32	55		0.75	6.2	0.25	50

In fact, the intercalation of Li in colloidal TiS_2 nanodiscs is a complex process involving not only the diffusion of Li ions within the nanodiscs but also the transport of Li ions at the interface of the nanodiscs and electrolyte solution. The rate of Li diffusion in the interlayer space of TiS_2 depends on the structural details of the nanodiscs, such as the interlayer distance, defect density, and the amount of intercalated Li according to the earlier experimental[65] and computational[67] studies on bulk crystal. The rate of interfacial transport of Li should depend on the structure of TiS_2 nanodiscs at the edges, solvent molecules and even the geometry of the nanodiscs on the surface of the substrate. Therefore, the time scales of the intercalation and deintercalation in TiS_2 nanodiscs observed here will not be a simple function of the diffusion coefficient and the radius of the nanodiscs. Nevertheless, we attempted to estimate the ‘effective’ diffusion

coefficient (D) of Li in TiS_2 nanodisc films using a continuum radial diffusion model assuming that the diffusion of Li within the TiS_2 lattice is the rate-limiting process and $\Delta A(t)/A$ is linear to the amount of intercalated Li. To further simplify the analysis, a single diffusion coefficient (D) independent of Li concentration was used. In the radial diffusion model, the time-dependent average concentration of Li normalized to its terminal concentration in a cylinder of radius r, $C(t,r)$, is expressed as follows, where a_n are the roots of Bessel function J_0.[68]

$$C(t,r) = 1 - \sum_{n}^{\infty} \frac{4}{a_n} \exp\left(-D \frac{{a_n}^2}{r^2} t\right)$$

The values of D were determined by fitting the normalized $|\Delta A(t)/A|$ to $C(t,r)$ as shown in Fig. 4.4. $|\Delta A(t)/A|$ fits well to $C(t,r)$ despite the limitation of the highly simplified model in describing the complex process. For the intercalation in r=80 nm nanodiscs with τ_1=2 s during the early cycles, the best fitting diffusion coefficient is $D=4\times10^{-12}$ cm^2/s. (See experimental section in this chapter for details.) For r=250 nm nanodiscs, the same analysis gives $D=1\times10^{-11}$ cm^2/s for the intercalation with τ_1=4 s. The values of D obtained above are much smaller than the diffusion coefficient of Li measured in bulk single crystalline TiS_2 measured via chronoamperometry ($D=10^{-9}$-10^{-8} cm^2/s) in a battery platform[41, 42], while they are similar to the upper range of D observed in microcrystalline TiS_2 layers ($D=10^{-11}$-10^{-13} cm^2/s) affected by the inter-domain diffusion.[43] However, considering the possible difference in the lattice parameters and the defect density between the colloidal nanodiscs and single crystalline bulk as well as

the increasing role of the transport of Li at the interface of the nanodiscs with decreasing size and electrolyte solution on the surface of a substrate, the observed difference in *D* is not surprising. Since the absorbance change is due to electron injection as mentioned, the optical change is sensitive to Faraday reaction with electron flows. Comparing with other electrochemical determination methods in Chapter II, the measuring of absorbance rules out non-Faraday reaction, which can contribute to increase the diffusion constant.

Interestingly, the values of *D* for TiS_2 nanodiscs from this study are more consistent with recently reported phase boundary propagation speed of 30-70 nm/s in MoS_2 nanosheets during Li intercalation,[49, 50] extracted from the analysis of TEM images. The root mean square displacement ($\sqrt{4Dt}$) from 2-dimensional diffusion is 63 nm for $D=1\times10^{-11}$ cm^2/s and t=1s, which is of the same order of magnitude as the reported phase boundary propagation speed in MoS_2 under Li intercalation[50].

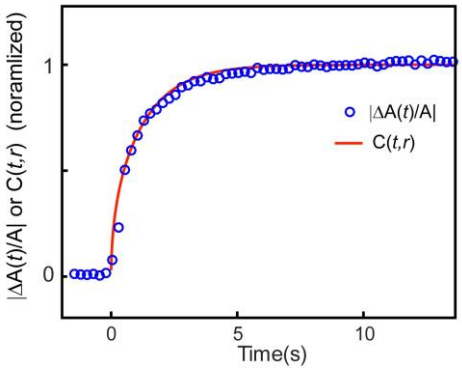

Figure 4.4 Fitting of |ΔA(*t*)/A| to the normalized average Li concentration in a cylinder of radius *r* at time *t*, C(*t*,*r*), from continuum radial diffusion model for the intercalation in TiS_2 nanodiscs with r=80 nm. The best fitting diffusion coefficient (D) is 4×10^{-12} cm^2/s.

A few interesting trends are observed in $\tau_1$values compiled in Fig. 4.2 (g, h). Firstly, τ_1 is smaller for deintercalation than intercalation, suggesting the lower overall kinetic barrier for the deintercalation process. The shorter τ_1 for the deintercalation may be in part due to the larger interlayer distance after the completion of Li intercalation, which would lower the barrier for Li diffusion within the lattice during the early phase of the deintercalation.[67] Secondly, both the intercalation and deintercalation become progressively slower as the intercalation/deintercalation cycle repeats. This can be interpreted as the result of the partially irreversible structural change creating defects during the repeated intercalation and deintercalation cycles, which increases the barrier for the Li diffusion. In fact, structural disorder or damage in various layered and non-layered materials used for Li battery created by the repeated charging and discharging has been previously reported,[69] which may also occur in colloidal TiS_2 nanodiscs.

In order to further examine the effect of repeated intercalation/deintercalation cycles on the kinetic barrier and the reversibility of the intercalation and deintercalation, $\Delta A(t)/A$ was measured with a modified scheme of the potential steps applied to the working electrode. Instead of using a simple potential switching between -1.1 V and 0.3 V, an open-circuit period was inserted after each -1.1 V. During the open-circuit periods, the removal of the thermodynamic driving force that kept Li ions within the host lattice results in the slower and partial deintercalation of Li. This is also the reason why a separate ex-situ quantification of the intercalated Li is difficult as mentioned earlier.

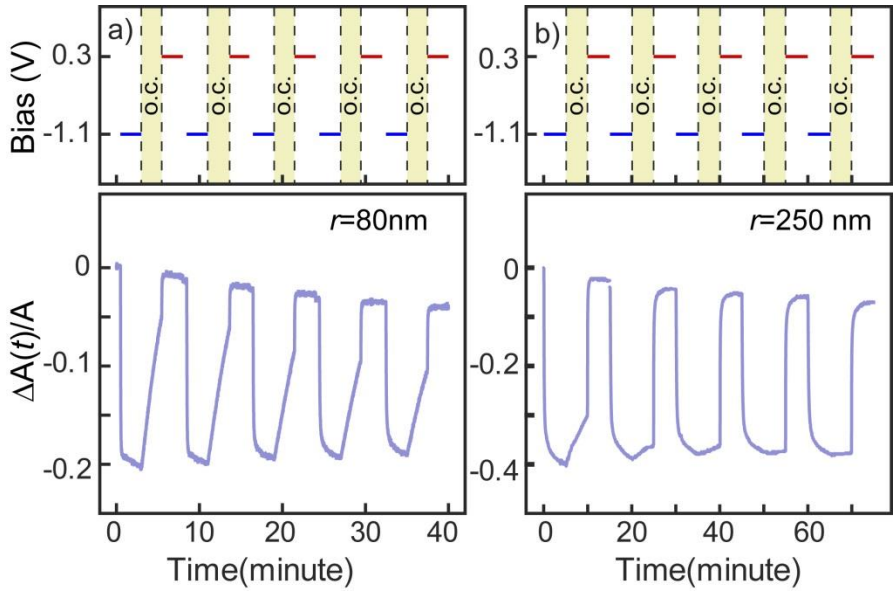

Figure 4.5 ΔA(*t*)/A at the absorption peak from the TiS2 nanodisc films of (a) *r*=80 nm and (b) *r*=250 nm under the modified electrode potential scheme. Open-circuit (o.c.) period was added between after -1.1 V. The electrode potential scheme is shown on top of each panel.

Fig. 4.5 shows the ΔA(*t*)/A obtained with the new electrode potential scheme for both TiS_2 nanodisc films. The top part of each panel shows the potential scheme applied to the working electrode. The recovery rate of ΔA(*t*)/A during the open-circuit period becomes slower as the potential cycle repeats in both nanodiscs, consistent with the increase of τ_1 as shown in Fig. 4.2 (g, h). The reversibility of the intercalation and deintercalation, on the other hand, is lower in the larger nanodiscs. The recovery of ΔA(*t*)/A during the open-circuit period stops after three cycles for *r*=250 nm while it continues for *r*=80 nm. This is also consistent with the faster increase of τ_1 with the cycle number for *r*=250 nm in Fig. 4.2(h), indicating more rapid increase of the barrier for the

intercalation and deintercalation processes. The dependence of the reversibility on the dimension of the nanodiscs has an important implication in the application of electrochemical intercalation for the dynamic control of the material properties in nanoscale layered materials. The higher irreversibility resulting in more 'non-volatile' behavior will be less desirable for the continuous tuning of the material properties, while it can be more advantageous for the applications requiring a switching behavior.

4.2.3 Calculation of dielectric constant in Li_xTiS_2

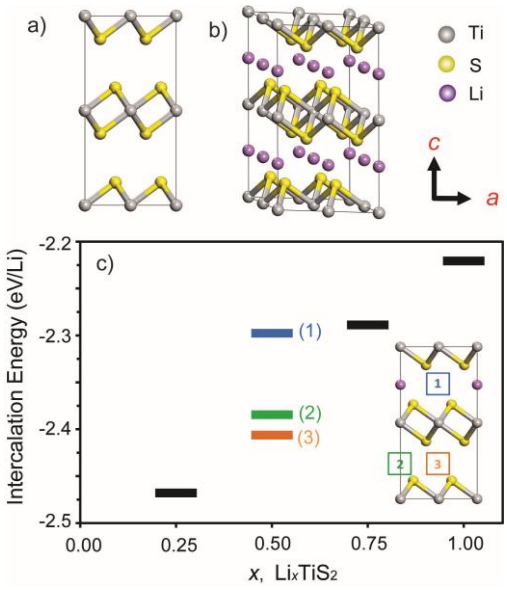

Figure 4.6 (a,b) 2×2×2 supercell of bulk TiS_2 (a) and $LiTiS_2$ (b). (c) Li intercalation energy in Li_xTiS_2 is given by $\left(E_{Li_xTiS_2} - \left(E_{TiS_2} + nE_{Li}\right)\right)/n$, where $E_{Li_xTiS_2}$, E_{TiS_2}, and E_{Li} are the calculated energies of lithiated TiS_2, non-lithiated TiS_2 and one Li metal atom, respectively. *n* is the number of lithium. Inset shows $Li_{0.25}TiS_2$ and colored squares represent O_h sites where Li can be placed when x=0.5

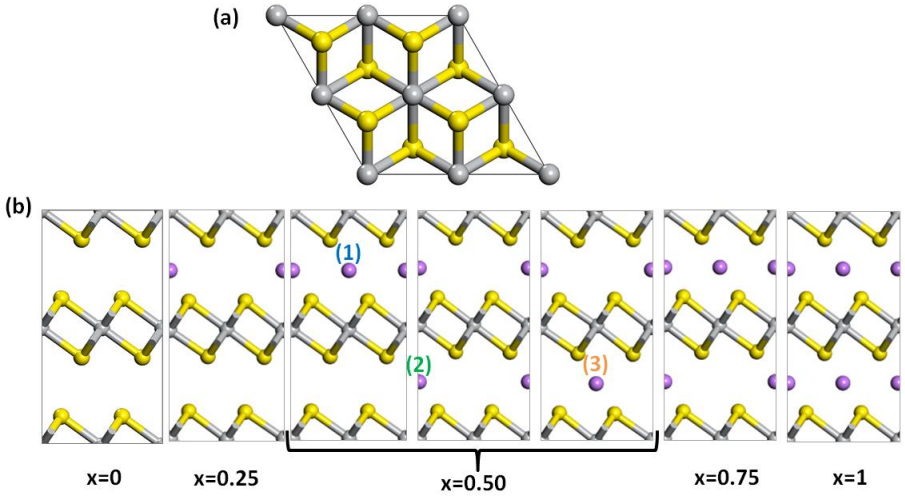

Figure 4.7 Li_xTiS_2 model. (a) top view of 2×2×2 supercell Li_xTiS_2 bulk; Li cannot be seen because they are in the same plane as Ti atoms. b) All different configurations for Li_xTiS_2. Gray, yellow, and pink spheres represent Ti, S, and Li atoms, respectively.

The validity of the optical measurement of the intercalation and deintercalation dynamics from $\Delta A(t)/A$ of the interband transition requires the continuous, preferably a linear function, of the amount of Li intercalated in TiS_2 nanodiscs. Here a computational approach is employed to evaluate the existence of such correlation. The optical absorption spectra of Li_xTiS_2 was calculated using a 2×2×2 Li_xTiS_2 bulk supercell as shown in Fig. 4.6 (a, b). The geometry of Li_xTiS_2 was first optimized at five different concentrations of lithium in the range of $0 \leq x \leq 1$. Three configurations were considered at x=0.50 and one at all other concentrations (Fig. 4.7). Li intercalation induced the expansion of the lattice along the vertical axis (about 8% of c for x=1) more substantially

than along the a-axis (<1% of *a*). These structural results are in good agreement with previous experimental and theoretical results.[70]

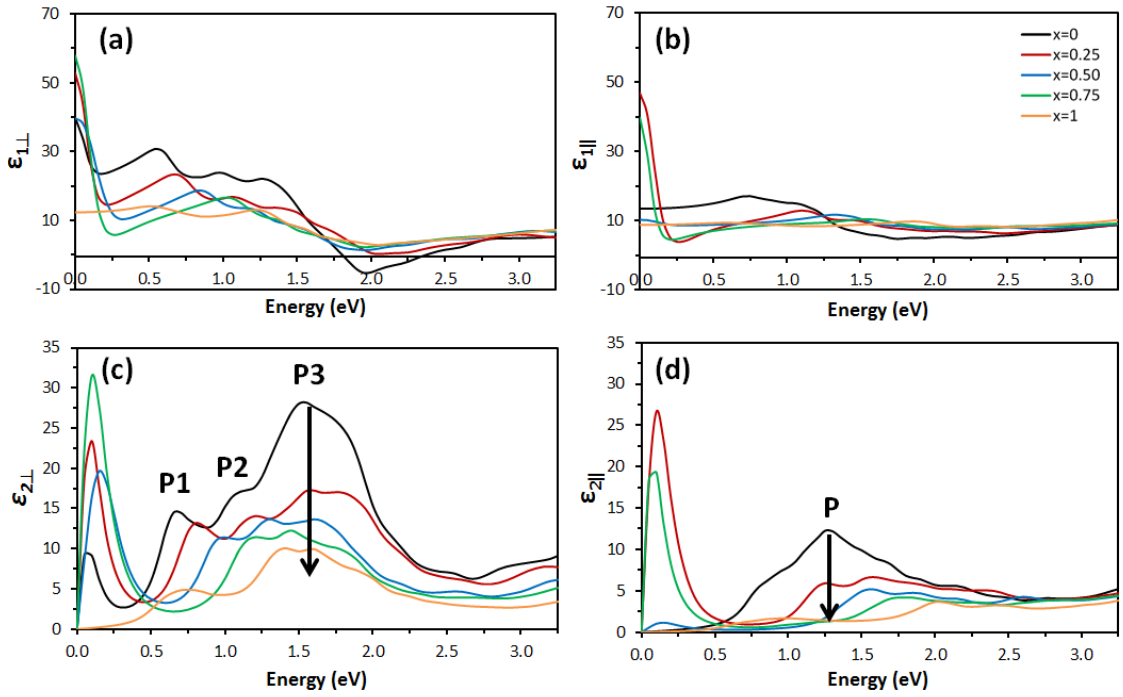

Figure 4.8 Complex dielectric function parallel ($\varepsilon_{\parallel}$) and perpendicular ($\varepsilon_{\perp}$) to the *c*-axis of TiS_2. Real and imaginary part of the dielectric function, (a, b) ε_1 and (c, d) ε_2 respectively, as a function of *x* in Li_xTiS_2. Arrows indicate the change of intensity at the main peaks as the concentration of lithium increases.

The imaginary part of the refractive index (k) representing the optical absorption intensity was computed from the calculated complex dielectric functions $\varepsilon_1 + i\varepsilon_2$(Fig. 4.8), using the equation $k^2 = \frac{1}{2}\left(\sqrt{\varepsilon_1^2 + \varepsilon_2^2} - \varepsilon_1\right)$ and the results are reported in Fig. 4.9 (a) and Fig. 4.10. For Li_xTiS_2, the component of k perpendicular to c-axis ($k_{\perp}$) is dominant over the parallel component ($k_{\parallel}$) in the energy range of 0.5-2.5 eV. In addition,

we used $k_\perp$ to find a correlation with x in Li_xTiS_2 because the absorption measured in the film of Li intercalated TiS_2 nanodiscs, lying flat on the substrate, is only contributed by the in-plane (i.e., perpendicular to *c*-axis) interband absorption.[33]

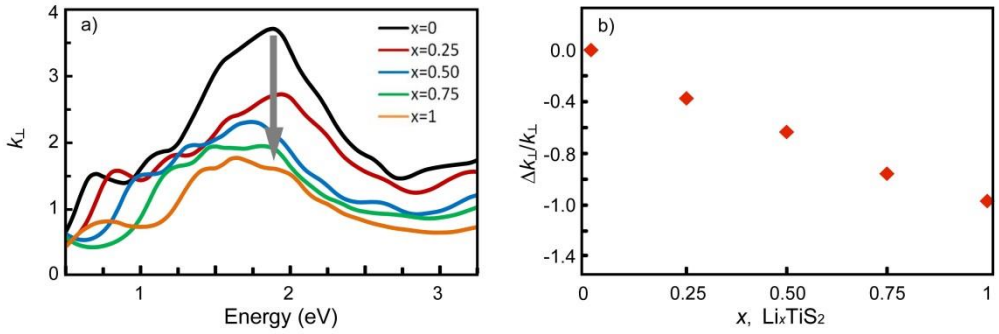

Figure 4.9 (a) Perpendicular component of the imaginary part of refractive index ($k_\perp$) as a function of *x* in Li_xTiS_2. Arrow indicates change of intensity at the main peak as the concentration of lithium increases. (b) Relative change of intensity of the main peak with respect to the non-lithiated case.

In Fig. 4.9(a), the peak centered at ~1.9 eV corresponds to the experimentally observed absorption peak at ~600 nm (2.06 eV) in Fig. 3.5. The intensity of this peak diminishes with increasing *x*, consistent with the experimental observation made in the present and earlier study.[33] Fig. 4.9(b) illustrates the relative change of the peak intensity of $k_\perp$ with respect to the non-lithiated case ($\Delta k_\perp/k_\perp$) as a function of *x* in Li_xTiS_2, which shows a nearly linear decrease with increasing *x*. This result indicates that the measurement of the fractional change in the interband absorption intensity, $\Delta A(t)/A$, can

be a reliable method to optically probe the dynamics of Li intercalation and deintercalation.

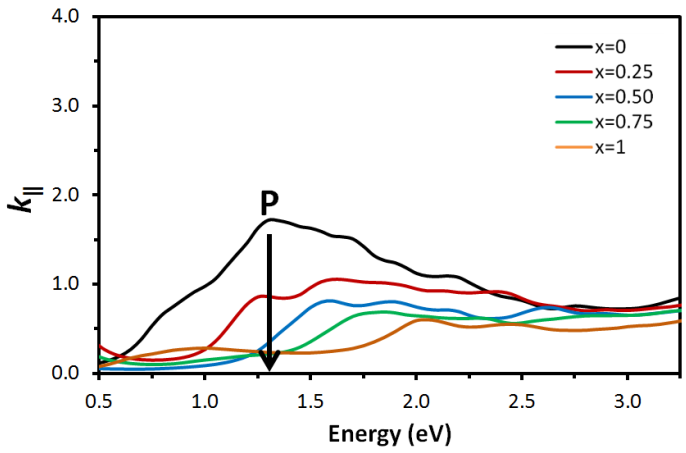

Figure 4.10 Parallel (out-of-plane) component of the imaginary part of refractive index ($k_{\|}$) as a function of x in Li_xTiS_2. Arrow indicates change of intensity at the main peak as the concentration of lithium increases.

4.3 Conclusions

In conclusion, we investigated the rapid dynamics of electrochemical Li intercalation and deintercalation in the layered TMD materials with nanoscale lateral dimension using the films fabricated with size-controlled colloidal TiS2 nanodiscs. In-situ optical spectroscopic method, detecting the changes in interband absorption intensity modified by Li intercalation, could conveniently probe the dynamics of intercalation and deintercalation varying with the size of the nanodiscs and also during the multiple

intercalation/deintercalation cycles affected by the partially irreversible changes in the host structure. The methodology for the measurement of the dynamics and the experimental results from this study will be valuable not only in obtaining the dynamic modulation of material properties but also for battery applications where understanding intercalation and deintercalation processes in nanoscale materials may allow better electrode designs utilizing the layered TMD materials with nanoscale lateral dimension.

4.4 Experimental methods

4.4.1 ΔA(*t*)/A dependence of electrode potential

The potential dependence experiment was conducted on a TiS_2 film fabricated with *r*=250 nm nanodiscs. The electrochemical cell was assembled as description in section 3.3. Five cycles of intercalation and deintercalation trials were applied in a sequence of -0.5 V, 0.3V; -0.7V, 0.3V; -0.9 V, 0.3V; -1.1 V, 0.3 V; -1.3 V, 0.3 V over Ag pseudo reference. Each segment of individual electrode potential was applied for five minutes. The results are shown before as Fig. 4.1.

4.4.2 Estimation of 'effictive' diffusion coefficient of Li in TiS_2 nanodiscs

The normalized experimental data of |ΔA(*t*)/A| was fit with the following expression of *C(t,r)*:

$$C(t,r) = 1 - \sum_{n}^{\infty} \frac{4}{a_n} \exp\left(-D \frac{{a_n}^2}{r^2} t\right)$$

$C(t,r)$ represents average concentration of Li normalized to its terminal concentration in a cylinder of radius r under 2-dimensional radial diffusion condition.[68]

For this fitting, the following 12 leading terms for a_n were used in the summation, which are the solutions of the Bessel function of the first kind $J_0(x)$:

2.405, 5.520, 8.654, 11.1975, 14.9309, 18.0711, 21.2116, 24.3525, 27.4935, 30.6346, 33.7758, 36.9171

4.4.3 DFT calculations

Spin polarized calculations were performed using the Vienna ab Initio Simulation Package (VASP),[71-73] with the projector-augmented wave (PAW) pseudopotentials[74, 75] to describe the electron-ion interactions. The Perdew-Burke-Ernzerhof generalized gradient approximations (GGA-PBE)[76] was employed as the exchange-correlation functional. The energy cut-off for the plane-wave basis was set to 500 eV. The partial occupancies were described with a 0.02 eV Gaussian smearing. The geometry optimizations and energy calculations were performed with a 4×4×2 Monkhorst-Pack[77] k-point grid, whereas a 8×8×4 k-point mesh was employed to calculate the absorption spectrum of bulk Li$_x$TiS$_2$. During the geometry optimization, the van der Waals interactions between TiS$_2$ layers were described using the zero-damping DFT-D3 method of Grimme.[78] The convergence criteria for electronic self-consistent iteration and ionic relaxation were set to 10^{-6} and 10^{-5} eV, respectively. Although techniques such as HSE06 and GW commonly yield electronic properties

closer to experimental values, relative variations of those properties using DFT-GGA are in good agreement as well.[79, 80]

Table 4.2 Optimized lattice parameters (a, b, and c) for different ratios and configurations of Li-intercalated in TiS_2 (Li_xTiS_2) in the supercell 2×2×2. a_u and c_u stand for the equivalent lattice parameters per unit cell.

x	Supercell			Ave. per unit cell*	
	a (Å)	b (Å)	c (Å)	a_u (Å)	c_u (Å)
0.00	6.792	6.792	11.411	3.396	5.705
0.25	6.777	6.784	11.783	3.390	5.892
0.50-(1)	6.792	6.792	11.827	3.396	5.914
0.50-(2)	6.766	6.786	12.183	3.388	6.092
0.50-(3)	6.779	6.787	12.135	3.392	6.068
0.75	6.791	6.798	12.188	3.397	6.094
1.00	6.806	6.806	12.221	3.403	6.110

* $a_u = (a+b)/4$; $c_u = c/2$

A unit cell of TiS_2 bulk with $P\bar{3}m1$ space group was used as initial configuration and then fully optimized. Optimized lattice parameters (a=3.389 Å and c=5.717 Å) were found in excellent agreement with previously reported theoretical and experimental results.[81, 82] The lattice parameters are summarized in Table 4.2. Regarding the lithium intercalation, three interstitial sites are available in the van der Waals gap of TiS_2 per unit cell; two tetragonal (T) and one octahedral (Oh). However, it has been reported that

lithium in Li_xTiS_2 occupy the Oh sites preferentially, larger intercalation energy, for $0<x<1$ following a reversible reaction without phase transition.[82-84] Therefore, we considered only this region and assumed that Li occupies only the Oh sites. Subsequently, a 2×2×2 supercell was built to allow several values of *x* between 0 and 1 to exist. Thus, different concentrations (*x*=0, 0.25, 0.50, 0.75, and 1; equivalent to 0, 2, 4, 6, or 8 Li per supercell) were used to examine the change of intensity on the optical absorption spectrum of Li_xTiS_2. The frequency dependent dielectric function, $\varepsilon(\omega) = \varepsilon_1(\omega) + i\varepsilon_2(\omega)$, was calculated using the independent-particle approximation as implemented within VASP.[85] 240 bands were used for these calculations. Due to symmetry, we can identify two independent components $\varepsilon_{\parallel} = \varepsilon_{zz}$ and $\varepsilon_{\perp} = (\varepsilon_{xx} + \varepsilon_{yy})/2$ that are parallel and perpendicular to the *c*-axis, respectively.

CHAPTER V

FUTURE ASPECTS

In the previous chapter, the dynamics of rapid lithium intercalation and deintercalation of 2D layered colloidal TiS_2 nanodiscs by in-situ optical measurement has been investigated. Using electrochemical device, the reversible optical absorption change was observed upon the immigration of lithium ions. And by monitoring real-time absorption change, the dynamics of ion diffusion was discussed.

To obtain stable and comparable data, the absorption change was mostly focused on very selective electrode potential conditions. Given the theoretical discussion and applied electrical bias dependence, the TiS_2-Li system has the potential for continuous adjustment of optical properties under modifying voltage control. The more delicate optical properties modulation of this system can be conducted and benefit the research of opto-electronics. Apart from investigated visible range, the enhancing absorption in near-IR range (>1400 nm) was clearly seen in TiS_2-Li system. This opens up the possibility of harvesting or inhibiting longer wavelength with plasmons.

The dynamics of intercalation and deintercalation of Li lead to swift performance of optical alteration through lateral dimension limited TiS_2 compared with larger TiS_2 and other layered transitional metal chalcogenide. The improved responding rate can be the key of designing and upgrading electrical components. The production of nanodiscs is currently incomparable with the manufacturing of graphene or MoS_2 films in nanometer thickness. Once the synthesis of nanodiscs is more mature and economically

available, it won't be far away from testing and utilizing nanodiscs in battery related application.

Due to low voltage output of lithium or lithium ion battery, TiS_2 is not the mainstream of cathode materials in current daily use.[86] But the convenient kinetics of Li-TiS_2 has been adapted for hybrid battery research with other anode material. For example, rechargeable Mg batteries are under research and development for its high volumetric capacity, low-cost and air stability,[87] while larger size and polarizability of Mg^{2+} is the hurdle to overcome for better ion diffusion. Since Li ion diffusion is favored in cathode material like TiS_2, Li^+ was used as the carrier in Mg-TiS_2 battery and this hybrid Mg^{2+}/Li^+ battery performed with long cycle life and high rate capability.[88] The existence of Li^+ also facilitates the intercalation of other guest species in TiS_2.

The electrochemical cell setup for Li-TiS_2 system is not limited to the only ion-host combination. The cell is based on reduction in the working electrode and rearrangement of double layer in the counter electrode. Thus the intercalation ion and receiving host dual can apply to more selections for in situ observation. In addition, the in situ monitoring property is not limited to optical change. This undoubtedly expands the application of the platform.

REFERENCES

(1) Smith, A. M.; Nie, S. *Accounts of Chemical Research* **2010,** *43,* 190.

(2) Wang, F.; Wang, Y.; Liu, Y.-H.; Morrison, P. J.; Loomis, R. A., *et al. Accounts of Chemical Research* **2015,** *48,* 13.

(3) Burda, C.; Chen, X.; Narayanan, R.; El-Sayed, M. A. *Chemical Reviews* **2005,** *105,* 1025.

(4) Alivisatos, A. P. *Science* **1996,** *271,* 933.

(5) Buhro, W. E.; Colvin, V. L. *Nat Mater* **2003,** *2,* 138.

(6) Tolbert, S. H.; Herhold, A. B.; Johnson, C. S.; Alivisatos, A. P. *Physical Review Letters* **1994,** *73,* 3266.

(7) Achermann, M.; Petruska, M. A.; Kos, S.; Smith, D. L.; Koleske, D. D., *et al. Nature* **2004,** *429,* 642.

(8) Kamat, P. V. *The Journal of Physical Chemistry C* **2008,** *112,* 18737.

(9) Talapin, D. V.; Lee, J.-S.; Kovalenko, M. V.; Shevchenko, E. V. *Chemical Reviews* **2010,** *110,* 389.

(10) Alivisatos, P. *Nat Biotech* **2004,** *22,* 47.

(11) Xia, F.; Wang, H.; Xiao, D.; Dubey, M.; Ramasubramaniam, A. *Nat. Photon.* **2014,** *8,* 899.

(12) Michalet, X.; Pinaud, F.; Lacoste, T. D.; Dahan, M.; Bruchez, M. P., *et al. Single Molecules* **2001,** *2,* 261.

(13) Hetsch, F.; Xu, X.; Wang, H.; Kershaw, S. V.; Rogach, A. L. *The Journal of Physical Chemistry Letters* **2011,** *2,* 1879.

(14) Sun, Z.; Martinez, A.; Wang, F. *Nat Photon* **2016,** *10,* 227.

(15) Yuan, H.; Wang, H.; Cui, Y. *Accounts of Chemical Research* **2015,** *48,* 81.

(16) Geim, A. K.; Grigorieva, I. V. *Nature* **2013,** *499,* 419.

(17) Gao, G.; Gao, W.; Cannuccia, E.; Taha-Tijerina, J.; Balicas, L., *et al. Nano Letters* **2012,** *12,* 3518.

(18) Kobayashi, K.; Yamauchi, J. *Phys. Rev. B* **1995,** *51,* 17085.

(19) Mak, K. F.; Lee, C.; Hone, J.; Shan, J.; Heinz, T. F. *Phys. Rev. Lett.* **2010,** *105,* 136805.

(20) Steinhoff, A.; Kim, J. H.; Jahnke, F.; Rösner, M.; Kim, D. S., *et al. Nano Lett.* **2015,** *15,* 6841.

(21) Koski, K. J.; Cha, J. J.; Reed, B. W.; Wessells, C. D.; Kong, D., *et al. J. Am. Chem. Soc.* **2012,** *134,* 7584.

(22) Wan, C.; Kodama, Y.; Kondo, M.; Sasai, R.; Qian, X., *et al. Nano Lett.* **2015,** *15,* 6302.

(23) Wan, C.; Gu, X.; Dang, F.; Itoh, T.; Wang, Y., *et al. Nat. Mater.* **2015,** *14,* 622.

(24) Starnberg, H. I.; Hughes, H. P. *J. Phys. C* **1987,** *20,* 4429.

(25) Jeong, S.; Yoo, D.; Ahn, M.; Miró, P.; Heine, T., *et al. Nat. Commun.* **2015,** *6*, 6763.

(26) Muller, G. A.; Cook, J. B.; Kim, H.; Tolbert, S. H.; Dunn, B. *Nano Lett.* **2015,** *15*, 1911.

(27) Whittingham, M. S. *J. Electrochemical Soc.* **1976,** *123*, 315.

(28) Whittingham, M. S. *Chem. Rev.* **2004,** *104*, 4271.

(29) Trevey, J. E.; Stoldt, C. R.; Lee, S.-H. *J. Electrochem. Soc.* **2011,** *158*, A1282.

(30) Seh, Z. W.; Yu, J. H.; Li, W.; Hsu, P.-C.; Wang, H., *et al. Nat Commun* **2014,** *5*.

(31) Winter, R.; Heitjans, P. *The Journal of Physical Chemistry B* **2001,** *105*, 6108.

(32) Ōnuki, Y.; Inada, R.; Tanuma, S.-i.; Yamanaka, S.; Kamimura, H. *J. Phys. Soc. Jpn.* **1982,** *51*, 880.

(33) Julien, C. M. *Mater. Sci. Eng. R-Rep.* **2003,** *40*, 47.

(34) Beal, A. R.; Nulsen, S. *Phil. Mag. B* **1981,** *43*, 965.

(35) Jeong, S.; Yoo, D.; Jang, J. T.; Kim, M.; Cheon, J. *J. Am. Chem. Soc.* **2012,** *134*, 18233.

(36) Reshak, A. H.; Kityk, I. V.; Auluck, S. *J. Chem. Phys.* **2008,** *129*, 074706.

(37) Klipstein, P. C.; Pereira, C. M.; Friend, R. H. Transport and Raman Investigation of the Group IV Layered Compounds and their Lithium Intercalates. In

Physics and Chemistry of Electrons and Ions in Condensed Matter; Acrivos, J. V.; Mott, N. F.; Yoffe, A. D., Eds. Springer Netherlands: Dordrecht, **1984**; p 552.

(38) Dahn, J. R.; Py, M. A.; Haering, R. R. *Can. J. Phys.* **1982,** *60,* 307.

(39) Küchler, W.; Heitjans, P.; Payer, A.; Schöllhorn, R. *Solid State Ionics* **1994,** *70,* 434.

(40) Whittingham, M. S. *Progress in Solid State Chemistry* **1978,** *12,* 41.

(41) Vaccaro, A. J.; Palanisamy, T.; Kerr, R. L.; Maloy, J. T. *J. Electrochem. Soc.* **1982,** *129,* 682.

(42) Kanehori, K.; Kirino, F.; Kudo, T.; Miyauchi, K. *J. Electrochem. Soc.* **1991,** *138,* 2216.

(43) Zehnder, D.; Deshpandey, C.; Dunn, B.; Bunshah, R. F. *Solid State Ionics* **1986,** *18/19,* 813.

(44) Ratnakumar, B. V.; Nagasubramanian, G.; Di Stefano, S.; Bankston, C. P. *J. Electrochem. Soc.* **1992,** *139,* 1513.

(45) Silbernagel, B. G. *Solid State Commun.* **1975,** *17,* 361.

(46) Li, X.; Zhu, H. *Journal of Materiomics* **2015,** *1,* 33.

(47) Wang, Y.; Ou, J. Z.; Balendhran, S.; Chrimes, A. F.; Mortazavi, M., *et al. ACS Nano* **2013,** *7,* 10083.

(48) Xiong, F.; Wang, H.; Liu, X.; Sun, J.; Brongersma, M., *et al. Nano Lett.* **2015,** *15,* 6777.

(49) Wang, L.; Xu, Z.; Wang, W.; Bai, X. *J. Am. Chem. Soc.* **2014,** *136,* 6693.

(50) Gao, P.; Wang, L.; Zhang, Y.; Huang, Y.; Liu, K. *ACS Nano* **2015,** *9,* 11296.

(51) Azhagurajan, M.; Kajita, T.; Itoh, T.; Kim, Y.; Itaya, K. *J. Am. Chem. Soc.* **2016**.

(52) Alliata, D.; Kötz, R.; Haas, O.; Siegenthaler, H. *Langmuir* **1999,** *15,* 8483.

(53) Campana, F. P.; Kötz, R.; Vetter, J.; Novák, P.; Siegenthaler, H. *Electrochemistry Communications* **2005,** *7,* 107.

(54) Rossi, D.; Han, J. H.; Yoo, D.; Dong, Y. T.; Park, Y., *et al. J. Phys. Chem. C* **2014,** *118,* 12568.

(55) Pavlishchuk, V. V.; Addison, A. W. *Inorg. Chim. Acta* **2000,** *298,* 97.

(56) Wu, S.; Buckley, S.; Jones, A. M.; Ross, J. S.; Ghimire, N. J., *et al. 2D Materials* **2014,** *1,* 011001.

(57) Zhang, Y.; Chang, T.; Zhou, B.; Cui, Y.; Yan, H., *et al. Nat. Nanotechnol.* **2014,** *9,* 111.

(58) Lezama, I. G.; Arora, A.; Ubaldini, A.; Barreteau, C.; Giannini, E., *et al. Nano Lett.* **2015,** *15,* 2336.

(59) Kumar, N.; Najmaei, S.; Cui, Q.; Ceballos, F.; Ajayan, P. M., *et al. Phys. Rev. B* **2013,** *87,* 161403.

(60) Malard, L. M.; Alencar, T. V.; Barboza, A. P. M.; Mak, K. F.; de Paula, A. M. *Phys. Rev. B* **2013,** *87,* 201401.

(61) Wang, Q. H.; Kalantar-Zadeh, K.; Kis, A.; Coleman, J. N.; Strano, M. S. *Nat. Nanotechnol.* **2012,** *7,* 699.

(62) Kim, H.; Kim, H.; Lee, J.; Lee, H.; Choi, D., *et al. ACS Nano* **2015,** *9,* 6854.

(63) Wang, H.; Yuan, H.; Hong, S. S.; Li, Y.; Cui, Y. *Chem. Soc. Rev.* **2015,** *44,* 2664.

(64) Mahler, B.; Hoepfner, V.; Liao, K.; Ozin, G. A. *J. Am. Chem. Soc.* **2014,** *136,* 14121.

(65) Yao, J.; Koski, K. J.; Luo, W.; Cha, J. J.; Hu, L., *et al. Nat. Commun.* **2014,** *5,* 6670.

(66) McCanny, J. V. *J. Phys. C* **1979,** *12,* 3263.

(67) Van der Ven, A.; Bhattacharya, J.; Belak, A. A. *Acc. Chem. Res.* **2013,** *46,* 1216.

(68) Crank, J. Diffusion in a cylinder. In *The Mathematics of Diffusion*; Oxford University Press: Bristol, England, **1975**; pp 73.

(69) Barré, A.; Deguilhem, B.; Grolleau, S.; Gérard, M.; Suard, F., *et al. J. Power Sources* **2013,** *241,* 680.

(70) Suslov, E. A.; Bushkova, O. V.; Sherstobitova, E. A.; Reznitskikh, O. G.; Titov, A. N. *Ionics* **2015,** 1.

(71) Kresse, G.; Hafner, J. *Phys. Rev. B* **1994,** *49,* 14251.

(72) Kresse, G.; Hafner, J. *Phys. Rev. B* **1993,** *47,* 558.

(73) Kresse, G.; Furthmüller, J. *Comput. Mater. Sci.* **1996,** *6,* 15.

(74) Blöchl, P. E. *Phys. Rev. B* **1994,** *50,* 17953.

(75) Kresse, G.; Joubert, D. *Phys. Rev. B* **1999,** *59,* 1758.

(76) Perdew, J. P.; Burke, K.; Ernzerhof, M. *Phys. Rev. Lett.* **1996,** *77,* 3865.

(77) Monkhorst, H. J.; Pack, J. D. *Phys. Rev. B* **1976,** *13,* 5188.

(78) Grimme, S.; Antony, J.; Ehrlich, S.; Krieg, H. *J. Chem. Phys.* **2010,** *132,* 154104.

(79) Shi, H.; Pan, H.; Zhang, Y.; Yakobson, B. I. *Phys. Rev. B* **2013,** *87,* 155304.

(80) Dong, L.; Namburu, R. R.; O'Regan, T. P.; Dubey, M.; Dongare, A. M. *J. Mater. Sci.* **2014,** *49,* 6762.

(81) Xu, C.; Brown, P. A.; Shuford, K. L. *RSC Adv.* **2015,** *5,* 83876.

(82) Dahn, J. R.; McKinnon, W. R.; Haering, R. R.; Buyers, W. J. L.; Powell, B. M. *Can. J. Phys.* **1980,** *58,* 207.

(83) Bernard, L.; Glaunsinger, W.; Colombet, P. *Solid State Ionics* **1985,** *17,* 81.

(84) Fernando, M.; Renato, C.; Arie, A. *J. Phys. Condens. Matter* **1997,** *9,* 3011.

(85) Gajdoš, M.; Hummer, K.; Kresse, G.; Furthmüller, J.; Bechstedt, F. *Phys. Rev. B* **2006,** *73,* 045112.

(86) Garsuch, A.; Herzog, S.; Montag, L.; Krebs, A.; Leitner, K. *ECS Electrochem. Lett.* **2012,** *1*, A24.

(87) Sun, X.; Bonnick, P.; Nazar, L. F. *ACS Energy Lett.* **2016,** *1*, 297.

(88) Gao, T.; Han, F.; Zhu, Y.; Suo, L.; Luo, C., *et al. Adv. Energy Mater.* **2015,** *5*, 1401507.

APPENDIX

The intercalation trial of Na^+ into TiS_2 nanodiscs was conducted. The setup of cell was similar in Section 3.4.2 with Li, switching the electrolyte solution from 0.1 M $LiClO_4$ to 0.1 M $NaClO_4$ in acetonitrile. The electrode potential scheme and $\Delta A(t)/A$ for five cycles at 600 nm of r=250 nm sample are shown in the upper and lower panel in Fig. A.1. The electrode potential applying pattern was composed of -1.1 V, open circuit and 0.3 V of five minutes each, with respect to intercalation, behavior without intercalation driving force and deintercalation. The $\Delta A(t)/A$ showed a similar trend in the first cycle of intercalation attempt as Li, while $\Delta A(t)/A$ was smaller and slower in dynamics as the sequence went. It suggests the irreversibility in optical modulation with the setup in 3.4.2.

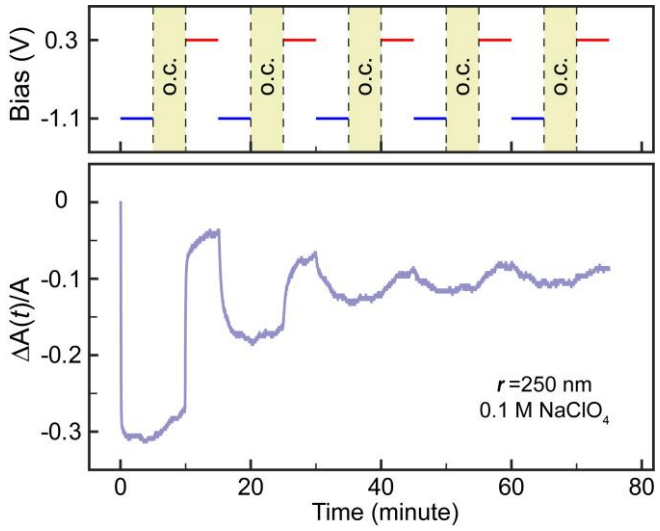

Figure A1 Data of Na^+ intercalation and deintercalation trial using the same setup as Li^+ of r=250 nm TiS_2 nanodiscs. The electrode potential apply during the five cycles is indicated in upper panel and $\Delta A(t)/A$ is shown in the lower panel.

Beside r=80 nm and r=250 nm mentioned in Chapter III and V, r=30 nm TiS_2 nanodiscs were also tested. The applying pattern, $\Delta A(t)/A$ and extracted τ_1 in intercalation of five cycles are shown in Fig. A.2. The setup of the cell was similar to section 3.4.2, but with r= 30 nm TiS_2 deposited on the ITO/glass. In each cycle the potential applying was arrange with five minutes of -1.1 V, 0.5 minutes of open circuit and 9.5 minutes of 0.3 V over the Ag pseudo reference. The data of $\Delta A(t)/A$ shows a large relative error, majorly due the low absorption of pre-intercalated TiS_2 film as well as lower absorption decrease upon intercalation. The decrease stability compared with larger TiS_2 mentioned may also contribute. It was tested that r=30 nm had a faster rate of oxidation and degradation, monitored by the absorption of nanodiscs film over time. The larger fluctuation of $\Delta A(t)/A$ leads to the greater uncertainty and error in time component fitting. Nonetheless, the τ_1 of the intercalation segment is reported and similar to the r=80 nm data.

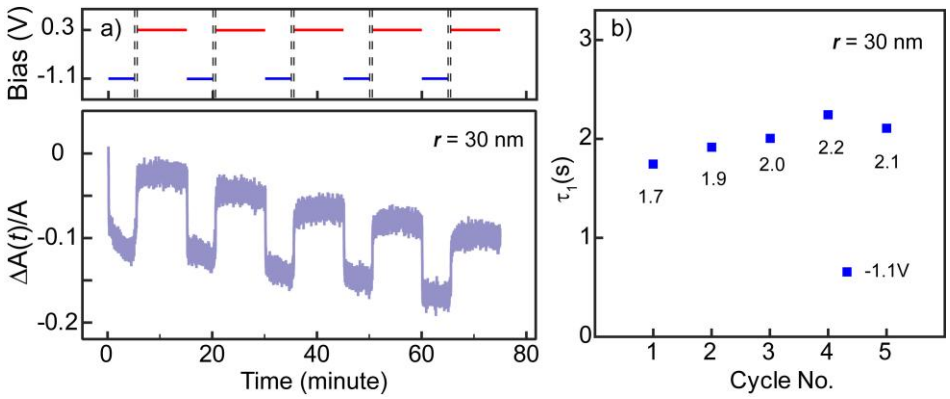

Figure A2 (a) The scheme of electrode potential applying and respective $\Delta A(t)/A$ with r= 30 nm TiS_2 nanodiscs in 0.1 M $LiClO_4$. (b) the value of τ_1 from only the intercalation part.